

# Defect-Free Perpendicular Diblock Copolymer Films: The Synergy Effect of Surface Topography and Chemistry

Xingkun Man,<sup>\*,†,‡</sup> Pan Zhou,<sup>§</sup> Jiuzhou Tang,<sup>||</sup> Dadong Yan,<sup>§</sup> and David Andelman<sup>\*,⊥,#</sup>

<sup>†</sup>Center of Soft Matter Physics and Its Applications and <sup>‡</sup>School of Physics and Nuclear Energy Engineering, Beihang University, Beijing 100191, China

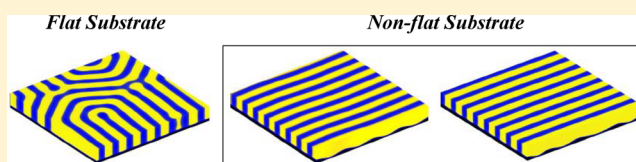
<sup>§</sup>Department of Physics, Beijing Normal University, Beijing 100875, China

<sup>||</sup>Beijing National Laboratory Molecular Sciences, Joint Laboratory of Polymer Science and Materials, Institute of Chemistry, and

<sup>⊥</sup>CAS Key Laboratory of Theoretical Physics, Institute of Theoretical Physics, Chinese Academy of Sciences, Beijing 100190, China

<sup>#</sup>Raymond and Beverly Sackler School of Physics and Astronomy, Tel Aviv University, Ramat Aviv 69978, Tel Aviv, Israel

**ABSTRACT:** We propose a directed self-assembly mechanism toward obtaining defect-free perpendicular lamellar phases of diblock copolymer (BCP) thin films. In our numerical study, a thin BCP film having a flat top surface is cast on a unidirectional corrugated solid substrate. The substrate is treated chemically and has a weak preference toward one of the two BCP components. Employing self-consistent field theory (SCFT), we find that there is an enhanced synergy between two substrate characteristics: its topography (geometrical roughness) combined with a weak surface preference. This synergy produces the desired perpendicular lamellar phase with perfect in-plane ordering. Defect-free BCP lamellar phases are reproducible for several random initial states and are obtained for a range of substrate roughness and chemical characteristics, even for a unidirectional multimode substrate roughness. Our theoretical study suggests possible experiments that will explore the interplay between unidirectional substrate corrugation and chemical surface treatment. It may lead to viable and economical ways of obtaining BCP films with defect-free lateral alignment.



## I. INTRODUCTION

Block copolymers (BCP) are a particular class of polymeric systems whose chain design is tightly connected with their functionality and applications. The BCP chains are composed of two or more chemically distinct blocks that are covalently tethered together. These systems spontaneously self-assemble into exquisitely ordered nanostructures with characteristic length scale in the range of a few nanometers to hundreds of nanometers.<sup>1</sup> For example, well-studied di-BCP melts produce a rich variety of three-dimensional morphologies including lamellae, hexagonally close-packed cylinders, BCC packing of spheres, and gyroid networks.<sup>2</sup> The wealth of these micro-phases continues to be intensely investigated by exploring chain architecture and chemical composition<sup>3–6</sup> or confining BCP films in finite geometries.<sup>7,8</sup>

Much advance has been done in recent decades on understanding the microphases of BCP in bulk and in film geometries. However, technology transfer into patterning applications crucially relies on controlling of structure and local alignment.<sup>9</sup> Such patterning technology might replace photolithography techniques in microelectronics, magnetic storage, solar cells, and novel optical devices.<sup>10,11</sup> Many techniques have been developed to attain such structural control, including chemical patterning of the substrate,<sup>12–14</sup> graphoepitaxy,<sup>15</sup> nanoimprint lithography,<sup>16,17</sup> and solvent annealing.<sup>18</sup>

The orientation of anisotropic phases (lamellae, cylinders) and their lateral (in-plane) ordering are two key factors in

achieving structural control of BCP thin films.<sup>19</sup> A perpendicular orientation with respect to the underlying substrate of BCP lamellae or cylinders is usually desirable for many materials and engineering applications.<sup>20</sup> It has been implemented successfully by varying the BCP<sup>21</sup> and substrate characteristics.<sup>22–27</sup> However, full control of the lateral ordering in industrial processes is still an ever-challenging issue. In particular, an unsolved problem is how to produce large defect-free arrays of BCP films in an economical and viable fashion, as is required in technological applications.<sup>28</sup>

Experimental techniques to orient lamellae in a perpendicular direction with respect to the substrate are well established. However, it is harder to control the film in-plane ordering. In order to produce a defect-free and perfect in-plane alignment, some experimental groups used corrugated substrates with a sinusoidal,<sup>29,30</sup> square-waved,<sup>31</sup> or sawtoothed<sup>32,33</sup> height variation. For example, Park et al.<sup>31</sup> investigated the self-assembly of BCP thin film on square-waved substrate. They reported that when the lamellar BCP film thickness is smaller than the corrugation amplitude, the in-plane alignment was found to be perpendicular to the long axis of the substrate trenches and exhibits almost perfect ordering with no in-plane defects. On the other hand, for thicker films, the substrate topography effect is weaker, resulting in a loss of the perfect in-

Received: August 19, 2016

Revised: October 12, 2016

Published: October 25, 2016

plane alignment and quite a number of defects. We note that in a recent and related (though preliminary) study<sup>34</sup> improved alignment of thicker lamellar forming BCP films was reported for blends of two di-BCPs having different block sizes.

It seems from the above-mentioned experimental studies<sup>29–32,34</sup> that, at present, there is only partial success in aligning defect-free lamellar forming BCP films as induced by substrate corrugation. On the theoretical side,<sup>35–40</sup> previous works have been mainly devoted to study the transition between parallel to perpendicular lamellar phases in the presence of a substrate. Most of these studies have been done in two dimensions and cannot address the important experimental issues related to in-plane alignment, which intrinsically requires a 3D study.

In the present work, we address in detail how substrate corrugation induces in-plane alignment of 3D BCP films. Our findings suggest that perfect in-plane alignment is achieved as a synergy of geometrical effects of unidirectional substrate trenches, together with a weak preference of the substrate toward one of the BCP components.

The outline of the paper is as follows. In the next section, we present the details of our model and explain how the BCP structure is obtained for corrugated substrates using self-consistent field theory (SCFT). In section III, we present our results, and in section IV we discuss the surface-induced alignment and its relation to current and future experiments. We also present in section IV our conclusions and some future prospects.

## II. MODEL

Our simulation setup is shown schematically in Figure 1. The simulations are performed in a three-dimensional (3D) box of

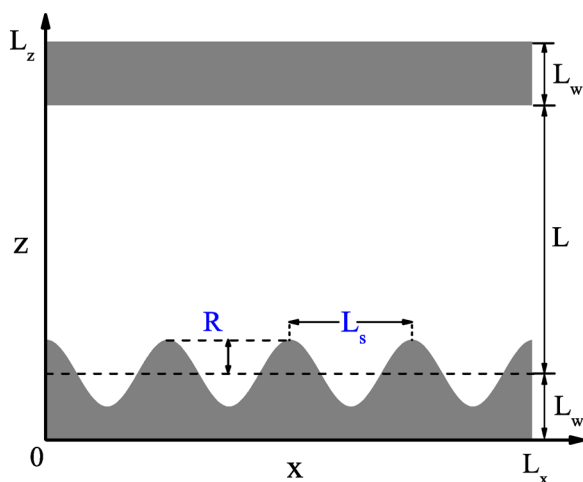


**Figure 1.** Schematic illustration of a BCP film confined between two surfaces. The 3D calculation box is of size  $L_x \times L_y \times L_z$ , and the averaged BCP film thickness is  $L = L_z - 2L_w$ , where  $L_w$  is the average wall thickness within the box. The corrugated substrate is described by a height function:  $h(x,y) = R \cos(q_s x)$ , with lateral wavenumber  $q_s = 2\pi/L_s$  and amplitude  $R$ . The substrate corrugation describes trenches that are translationally invariant in the  $y$ -direction.

size  $L_x \times L_y \times L_z$ . The technical details of using masking method to treat the boundaries can be found in ref 40 and will not be repeated here. The top surface is taken as a flat interface in order to mimic the BCP surface with air, while the bottom surface is sinusoidally corrugated along the  $x$ -direction and

translationally invariant along the  $y$ -direction. The substrate height function is then written as

$$h(x, y) = R \cos(q_s x) \quad (1)$$

and describes periodic surface trenches having a single  $q$ -mode along the  $x$ -direction with wavenumber  $q_s$ , periodicity  $L_s = 2\pi/q_s$ , and amplitude  $R$ . The average thickness of the BCP film,  $L$ , is averaged over the corrugation of the substrate (see Figure 1). Although the present study is restricted to simple sinusoidal corrugations, our simulations can equally be applied to other types of surface corrugation such as sawtoothed, square-wave, etc.

Self-consistent field theory (SCFT) is used to investigate the lamellar phase of A/B di-BCP, with a natural periodicity in our thin film geometry,  $L_0 = 2\pi/q_0$ . The 3D BCP film is confined between a flat top surface and a corrugated bottom one as defined in eq 1. We consider a melt of  $n_c$  chains, each composed of  $N = N_A + N_B$  monomers. The A-component molar fraction is  $f = N_A/N$ , and that of the B-component is  $1 - f$ . Hereafter, we concentrate on symmetric di-BCP, i.e.,  $f = 0.5$ . All lengths are rescaled with the chain radius of gyration,  $R_g = \sqrt{Nb^2/6}$ , where  $b$  is the Kuhn length taken for simplicity to be the same for the two blocks.

The Flory–Huggins parameter between the A and B monomers (in units of  $k_B T$ ) is  $\chi_{AB}$ , and  $u = N\chi_{sA} - N\chi_{sB}$  is the relative interaction between the substrate and the A/B components, where  $\chi_{sA}$  ( $\chi_{sB}$ ) is the interaction parameter between the substrate and the A (B) component. This choice means that a positive  $u$  induces substrate preference of the A component. A detailed formulation of the numerical procedure (pseudospectral method with FFTW) and its implementation to SCFT modeling of BCP systems can be found elsewhere.<sup>41–43</sup>

The SCFT formulation gives the local density for the A and B components,  $\phi_A(\mathbf{r})$  and  $\phi_B(\mathbf{r})$ , respectively. There are two orientations of the BCP film with respect to the substrate, and they are shown schematically in Figure 2. The parallel orientation is denoted  $L_{\parallel}$  and is shown in Figure 2a, while the perpendicular one is denoted as  $L_{\perp}$ . The  $L_{\perp}$  phase can be further divided into two orientations,  $L_{\perp}^1$  and  $L_{\perp}^2$ , which are orthogonal to each other as shown in Figure 2b and Figure 2c. Whereas  $L_{\perp}^1$  is orthogonal to the trench long axis, the  $L_{\perp}^2$  ordering is parallel to the trenches. The BCP films in our study are in contact with a uniaxial corrugated substrate that has a small preference toward one of the two BCP components. In the next section we will show under what conditions it is possible to obtain a defect-free  $L_{\perp}$  phase.

## III. RESULTS

**A. Defect-Free Thin Film of Lamellar BCP.** The structure of the BCP film is obtained via the SCFT method applied to the weak segregation,  $N\chi_{AB} = 12$ . For this  $N\chi_{AB}$  value, the BCP natural periodicity in our thin film geometry is  $L_0 = 3.35$  (in units of  $R_g$ ). We performed simulations at this temperature (close to ODT) because it is much easier at this temperature to anneal away the in-plane defects. The BCP film of thickness  $L = 3 = 0.9L_0$  is simulated inside a 3D box of cross-section  $L_x \times L_y = 26.8 \times 26.8 = 8L_0 \times 8L_0$  and of height  $L_z = 4.0 = 1.2L_0$ . Figure 3 shows the thermal equilibrated state of a BCP film that is cast on neutral substrate,  $u = 0$ . In (a), the substrate is flat ( $R = 0$ ), while in (b)–(e) the substrate is corrugated with  $R = 0.25$  and has a decreasing periodicity:  $L_s = 2\pi/q_s = 26.8 =$

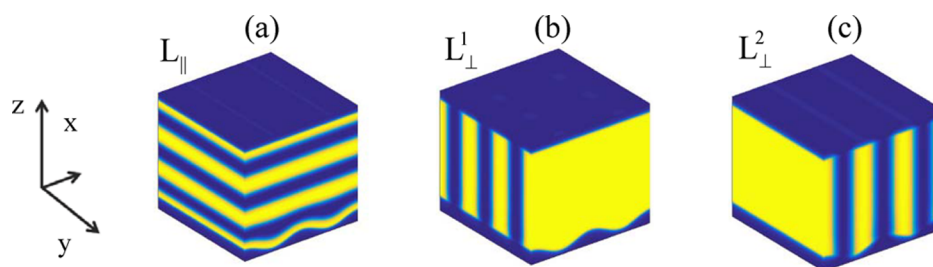


**Figure 2.** Three orthogonal lamellar orientations for BCP films in contact with a bottom substrate that is sinusoidally corrugated. A-rich regions are denoted by yellow and B-rich by blue. In (a) the lamellar orientation is parallel to the substrate, and the phase is denoted as  $L_{\parallel}$ , while in (b) and (c) we show the two orientations that are perpendicular to the substrate (and to each other). In (b) the lamellae are perpendicular to the long axis of the substrate trenches, and the phase is denoted as  $L_{\perp}^1$ . In (c) the lamellae are parallel to the trench long axis, and the phase is denoted as  $L_{\perp}^2$ .

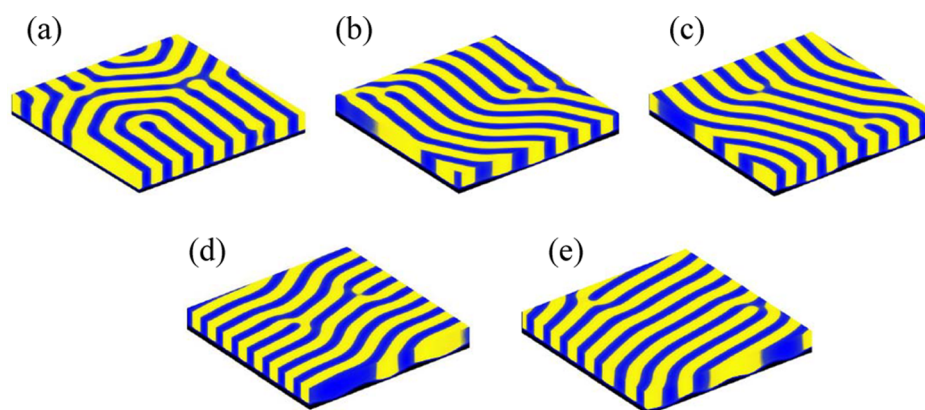


**Figure 3.** 3D BCP films of thickness  $L = 3.0 = 0.9L_0$  inside a simulation box of size,  $L_x = L_y = 26.8 = 8L_0$ , and  $L_z = 4.0 = 1.2L_0$ . Both the top flat surface and the bottom substrate are neutral,  $u = 0$ . In (a), the substrate is flat, while in (b)–(e) it is corrugated with  $R = 0.25$  and with corrugation periodicity,  $L_s = 26.8 = 8L_0$  in (b),  $L_s = 13.4 = 4L_0$  in (c),  $L_s = 8.9 = 2.7L_0$  in (d), and  $L_s = 6.7 = 2L_0$  in (e). All lengths are rescaled by the chain radius of gyration,  $R_g$ . In all parts a–e, the resulting lamellar phase is perpendicular to the substrate and has many in-plane defects.

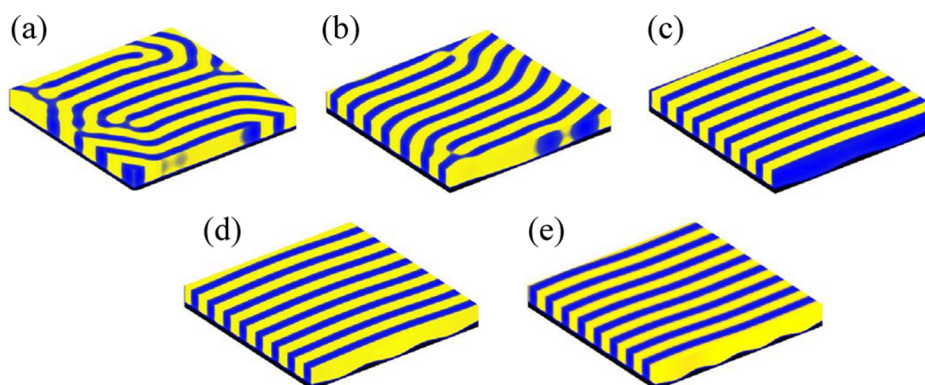


**Figure 4.** 3D BCP films of thickness  $L = 3.0 = 0.9L_0$  inside the same simulation box as in Figure 3. The top flat surface is neutral, and the bottom substrate has a small preference,  $u = 0.5$ . In (a), the substrate is flat ( $R = 0$ ), while in (b)–(e), it is corrugated with  $R = 0.25$ . The lamellar phase has a perpendicular orientation with respect to the substrate, with in-plane defects in (a) and in (b), where  $L_s = 8L_0$ . The lamellar structure is a defect-free  $L_{\perp}^1$  (orthogonal to the trench axis) in (c)–(e), with  $L_s = 4L_0$  in (c),  $L_s = 2.7L_0$  in (d), and  $L_s = 2L_0$  in (e).

$8L_0$  in (b),  $L_s = 13.4 = 4L_0$  in (c),  $L_s = 8.9 = 2.7L_0$  in (d), and  $L_s = 6.7 = 2L_0$  in (e). For neutral substrates that are either flat or corrugated, the BCP film forms a  $L_{\perp}$  phase but has many defects with no in-plane alignment. For the same neutral and corrugated substrate, we repeated the simulations with different choices of random initial conditions. Convergence is always obtained to a  $L_{\perp}$  phase with a multitude of defects. As the initial conditions are changed, defects are always found inside the BCP film, but at different and randomly distributed positions.

In Figure 4, we repeat the same simulations as in Figure 3, but with a small added substrate preference,  $u = 0.5$  (in units of

$k_B T$ ). Note that  $u \ll N\chi_{AB}$  is chosen to be small enough so that it does not induce the  $L_{\parallel}$  phase.<sup>40</sup> For the flat substrate in Figure 4a and the corrugated substrate with large periodicity of  $L_s = 8L_0$  in Figure 4b, we obtain an  $L_{\perp}$  phase with many in-plane defects. As the corrugation periodicity decreases (while keeping  $u$  and  $R$  constant), a defect-free  $L_{\perp}^1$  is found in Figure 4c–e, where  $L_s$  varies between  $4L_0$  and  $2L_0$ .

Two conclusive remarks, supported by Figure 4, can be made at this stage. (i) In order to get a perfect (defect-free)  $L_{\perp}$  phase, the substrate corrugation periodicity should lie in the range of  $2L_0 \leq L_s \leq 4L_0$  when the other setup parameters are  $u = 0.5$ ,

$R = 0.25 \approx 0.07L_0$ , and  $L = 0.9L_0$ . (ii) The stability of the defect-free  $L_{\perp}$  crucially depends on a moderate surface preference, parametrized by a small  $u$  value of the corrugated substrate.

The defect-free  $L_{\perp}$  phase can be reproduced in an entire range of the corrugation amplitude,  $R$ , and periodicity,  $L_s$ , as long as the substrate exhibits a small preference toward one of the BCP components and its corrugation is unidirectional. An example of a perfectly aligned  $L_{\perp}^1$  is shown in Figure 5 for



**Figure 5.** Effect of the substrate roughness amplitude,  $R$ , on the 3D BCP film structure. In (a), (b), and (c), the amplitude  $R$  is 0.15, 0.35, and 0.45, respectively. The film and simulation box are the same as in Figure 4. In all figure parts, the substrate is corrugated with periodicity  $L_s = 4L_0$ , and the resulting lamellar phase in all cases is defect-free  $L_{\perp}^1$ .

$L_s = 4L_0$  and  $u = 0.5$ . Further checks showing similar behavior were also performed for  $L_s = 2L_0$  without presenting them here explicitly. The  $L_{\perp}$  phase shown in Figure 5 is defect-free for the same range in corrugation amplitude, varying between  $R = 0.15$  in Figure 2a to 0.45 in Figure 2c.

From the presented results, a prediction with experimental consequences emerges. It suggests that the perfect  $L_{\perp}$  alignment is induced by the substrate roughness,  $R \geq 0.15$  ( $\approx 0.05L_0$ ), but is not sensitive to the specific value of  $R$ . The defect-free  $L_{\perp}$  structure can be reproducible and was repeatedly obtained for several different random initial conditions of the BCP film, always in contact with the same corrugated substrate.

**B. Conditions for the Stability of the Perpendicular Phase.** In order to understand why we obtain defect-free  $L_{\perp}$  phases, the relative stability of lamellar phases with the three orthogonal orientations ( $L_{\parallel}$ ,  $L_{\perp}^1$ , and  $L_{\perp}^2$ ) is studied by comparing their free energies. The effect of surface preference is addressed more quantitatively in Figure 6, where the transition between  $L_{\perp}$  and  $L_{\parallel}$  is shown in the  $(u, q_s R)$  plane. We use larger  $u$  values (between 3.0 and 4.2) in order to compare the present 3D study (red line) with the previous two-dimensional (2D) (dashed black line) study of ref 40, where

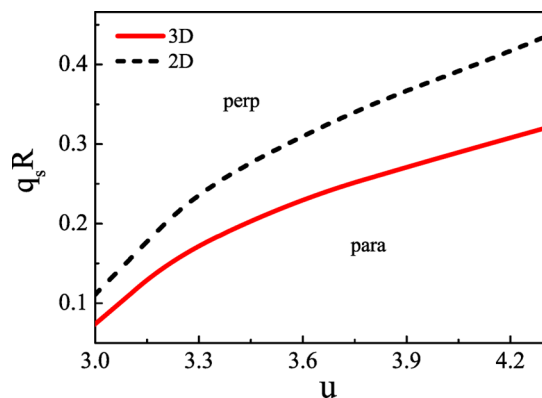


**Figure 6.** Parallel ( $L_{\parallel}$ ) to perpendicular ( $L_{\perp}$ ) phase transition in the  $(u, q_s R)$  plane. A comparison is shown between a 3D (red solid line) and a 2D (dashed black line) system. In 3D, the perpendicular phase is the  $L_{\perp}^1$  and has an extended region of stability as compared to 2D. The top flat surface is neutral and  $N\chi_{AB} = 25$ .

the BCP was taken in the strong segregation regime,  $N\chi_{AB} = 25$ . As can be seen in Figure 6, the region of stable  $L_{\perp}$  is quite extended, while the stabilization of the  $L_{\parallel}$  phase requires large  $u$  values. For the weaker segregation regime, such as  $N\chi_{AB} = 12$  that is used in most of the present study, the stability of the  $L_{\perp}$  is even further enhanced.

Note that in 2D there is only one perpendicular phase to the substrate, while in 3D there are two perpendicular orientations: the  $L_{\perp}^1$  phase that is orthogonal to the trenches, and the  $L_{\perp}^2$  whose orientation is parallel to the trenches (see Figure 2). With infinite trenches in the  $y$ -direction, the latter  $L_{\perp}^2$  phase in 3D resembles the  $L_{\perp}$  phase in 2D. As will be shown below, the  $L_{\perp}^1$  is more stable than  $L_{\perp}^2$ , resulting in a larger region in Figure 6 occupied by the stable 3D perpendicular phase in the phase diagram, as compared with the 2D case.

In Figure 7, we show the relative stability of the two perpendicular orientations,  $L_{\perp}^1$  and  $L_{\perp}^2$ , for a fixed and relatively

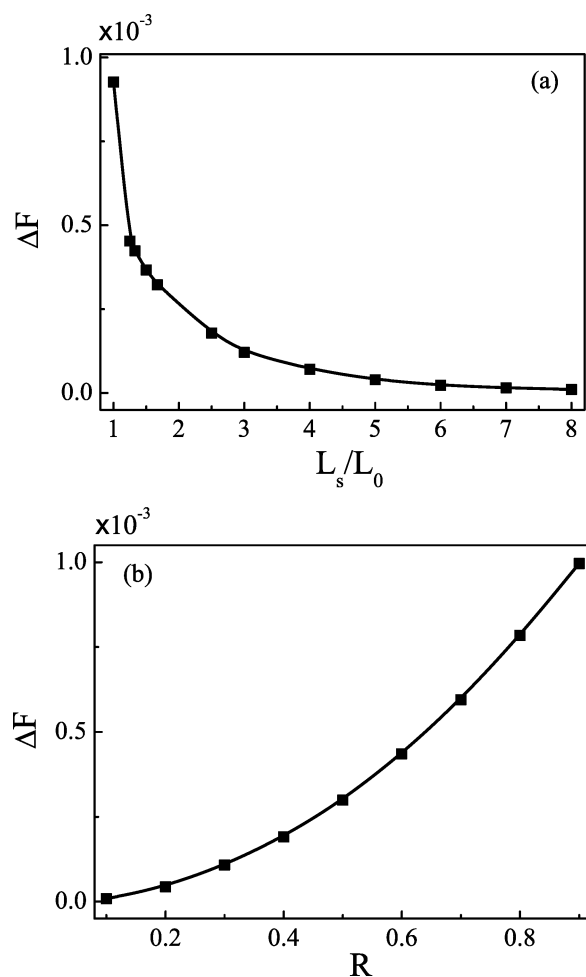


**Figure 7.** Free energy difference per unit volume,  $\Delta F = F_{\perp}^2 - F_{\perp}^1$ , in units of  $k_B T$  is shown to be (a) a decreasing function of  $L_s/L_0$  and (b) an increasing function of  $R$ . All other parameters are as in Figure 4.

small value of the substrate preference,  $u = 0.5$ . The free energy difference per unit volume,  $\Delta F = F_{\perp}^2 - F_{\perp}^1$  (in units of  $k_B T$ ), is plotted as a function of the periodicity ratio,  $L_s/L_0$  in (a) and as a function of the substrate amplitude  $R$  in (b). Since we are in the weak segregation regime ( $N\chi_{AB} = 12$ ), the free energy difference between the two orientations is small, of order  $10^{-3}$  (in units of  $k_B T$  per unit volume). As  $\Delta F$  is positive for the

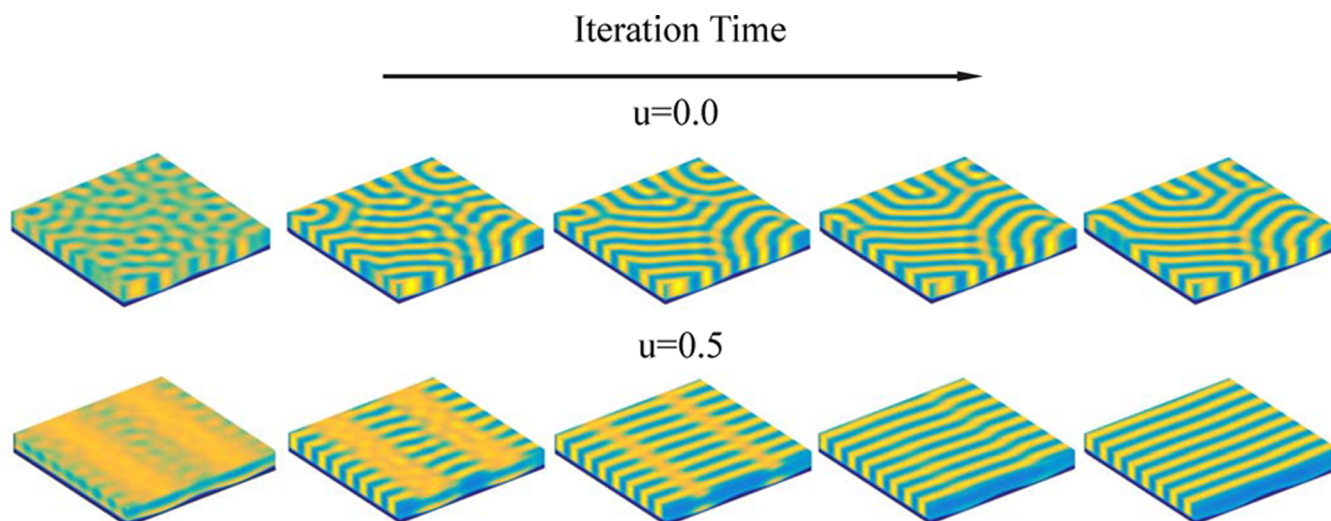


**Figure 8.** Temporal evolution of the BCP lamellar phase along the SCFT iteration time axis. The top panel is for a BCP thin film in contact with a neutral sinusoidal substrate,  $u = 0$ , while the bottom one is for a substrate with a weak preference to one of the BCP components,  $u = 0.5$ . Other parameters are  $L_s = 4L_0$ ,  $R = 0.25$ ,  $L_x = L_y = 26.8 = 8L_0$ , and  $L_z = 4.0 = 1.2L_0$ . The minimum and maximum values of the BCP density are adjusted for each iteration time, in order that the modified color code will give a better representation of the structural evolution.

entire range of parameters, the  $L_{\perp}^1$  phase (i.e., perpendicular to the trenches) is the most stable one. In the limit of  $R \rightarrow 0$  and  $L_s/L_0 \rightarrow \infty$ , the corrugated substrate approaches a flat one and  $\Delta F$  becomes vanishingly small.

To elucidate the effect of substrate preference in enhancing the lateral ordering, we present in Figure 8 sequential snapshots of BCP lamellae along the SCFT iteration time axis. Although there is no real dynamics in this SCFT time axis, it is instructive to see the clear difference between the equilibrated BCP thin film in contact with a *neutral* substrate ( $u = 0$ , top panel), as opposed to a substrate with a *small preference* ( $u = 0.5$ , bottom panel).

For a neutral substrate and at early times, the in-plane orientation of perpendicular lamellae is completely random and has no coupling with the substrate topography. As the iterations proceed, domains with different orientations grow and eventually merge, leading to a large number of defects. On the other hand, for a substrate with a weak preference (nonzero  $u$  in the bottom panel of Figure 8), most regions of the BCP thin film are in the parallel phase. This result strongly limits the orientation of the perpendicular lamellae around the crests of the surface. Then, these perpendicular domains grow and eventually merge, resulting in a perfect perpendicular lamellar phase.

**C. Multimode Corrugated Substrates.** So far, the corrugated substrate was characterized by a single unidirectional sinusoidal mode for the entire simulation box. In order to model the experimental situation where substrates have an entire distribution of  $q$ -modes, we present in Figure 9 an example of a BCP film in contact with a multimode corrugated substrate. As our simulation box has the size of about eight lamellar periodicities,  $L_x = L_y \simeq 8L_0$ , we cannot simulate a real multimode random substrate. Instead, we use a substrate composed of four sections, each with a different periodicity between  $1.5L_0$  and  $3.0L_0$  (see Figure 9). An important point to consider is that the substrate unidirectionality is strictly observed as well as the weak value of its preference parameter,  $u \gtrsim 0$ . Keeping these points in mind, Figure 9 indeed shows that the BCP alignment is not sensitive to such a choice of a

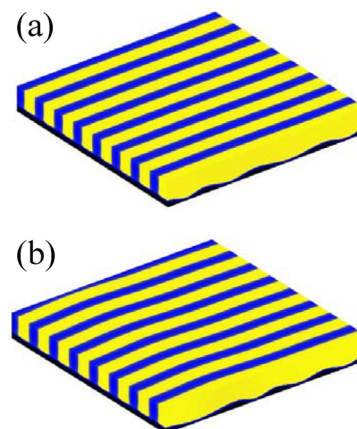


**Figure 9.** 3D BCP film in contact with a multimode sinusoidal substrate. The film and simulation box are the same as in Figure 4. The amplitude of the corrugated substrate is  $R = 0.25$ , while the corrugation periodicity is a combination of four different periodicities. In (a) the four periodicities are  $1.5L_0$ ,  $2.0L_0$ ,  $2.8L_0$ , and  $1.7L_0$ , and in (b) they are  $3.0L_0$ ,  $1.5L_0$ ,  $1.9L_0$ , and  $1.6L_0$ . Both lamellar phases are defect-free  $L_{\perp}^1$ .

multimode substrate. The obtained BCP phase is still a defect-free  $L_{\perp}^1$ .

#### IV. DISCUSSION AND CONCLUSIONS

In this paper we proposed a directed self-assembly scheme to obtain defect-free perpendicular BCP lamellar phases by manipulating both the geometrical roughness and chemical preference of the underlying corrugated substrate. Our results suggest that there is an enhanced synergy between these two important substrate properties as long as we maintain unidirectional substrate corrugations and a small surface preference. However, the two surface perturbations cannot be too large. If a large chemical preference is introduced, it will destabilize the  $L_{\perp}^1$  phase (and stabilize the parallel phase,  $L_{\parallel}$ ). Similarly, a large  $q_s R$  values will cause pronounced deformations of the  $L_{\perp}^1$ , with potential defects close to the corrugated substrate.<sup>40</sup>

In terms of the defect-free  $L_{\perp}$  phase, our results are robust as can be seen in Figures 3–5. Changes in the periodicity  $L_s$  and amplitude  $R$  of the substrate corrugation do not affect the alignment, as long as the unidirectional corrugation is moderate and the substrate preference parameter is small. Furthermore, the defect-free  $L_{\perp}$  phase is obtained even for multimode corrugated substrates as shown in Figure 9. Another reason for the claimed robustness is that the defect-free  $L_{\perp}$  phase is obtained for different choices of the random initial condition of the film structure, mimicking a film preparation above the ODT or a disordered BCP solution that is spin-cast onto the substrate.

As in any numerical scheme, we are limited by the system finite size. To check our predictions, we also simulated (without showing results) larger lateral system sizes of about  $10L_0$ , while the film thickness was kept the same as before,  $L = 0.9L_0$ . As long as  $2L_0 \leq L_s \leq 4L_0$ , we still obtain the perfect  $L_{\perp}$  phase. Although our simulation results are indicative, they are not completely sufficient to predict that a similar combination of substrate topography and chemical preference can induce defect-free  $L_{\perp}$  for systems with much larger lateral size, as is required in experiments. This is a deficiency of all simulation schemes as the simulation box has a finite size that is often smaller than the experimental relevant sizes. In addition, as experiments have reported a dependence of the film orientation on its thickness,<sup>44</sup> we conjecture that a perfect  $L_{\perp}$  phase of different thicknesses or sizes requires different values of the roughness parameters ( $q_s$  and  $R$ ) and preference parameter,  $u$ . This conjecture has yet to be confirmed in future studies.

In a fraction of our simulations, instead of obtaining a defect-free  $L_{\perp}^1$  phase, the system converged toward a tilted  $L_{\perp}$  phase. These tilted  $L_{\perp}$  lamellae have a perfect perpendicular orientation with respect to the substrate and are aligned with a small tilt angle with respect to the in-plane direction of the  $L_{\perp}^1$  phase, but still without any in-plane defects. We note that tilted lamellar phases have also been found in experiments.<sup>31,33</sup> Park et al.<sup>31</sup> reported that symmetrical PS-*b*-PMMA can form tilted lamellar phases without in-plane defects, when the BCP thickness is rather small and comparable to the magnitude of corrugation. Hong et al.<sup>33</sup> showed that the long axis of the BCP cylinders is parallel to the substrate. Furthermore, the in-plane cylindrical orientation is overall perpendicular to the trenches, with a small tilt angle of about  $1^{\circ}$ – $3^{\circ}$ .

We find that the free energy of titled lamellar phase is somewhat higher than the free energy of the perfect nontilted one. However, the energy difference is very small, on the order of  $10^{-3}k_B T$ , which is too small to represent a real penalty that will drive the system from the tilted phase to the perfect one. Our simulations suggest that increasing the ratio,  $L_z/R$ , between film thickness ( $L_z$ ) and the corrugation magnitude ( $R$ ) can enhance the lateral alignment of the lamellar phase. We note that  $L_z/R \approx 1$  in experiments,<sup>31</sup> while it is  $\approx 10$  in our simulations.

The tendency of the  $L_{\perp}$  phase to align in the  $L_{\perp}^1$  direction that is orthogonal to the trenches (as compared to the parallel one,  $L_{\perp}^2$ ) is shown in Figure 7. From the figure it is observed that the free energy difference  $\Delta F = F_{\perp}^2 - F_{\perp}^1$  is always positive. This observation is consistent with previous theoretical findings and experiments.<sup>31,33,34</sup> Pickett et al.<sup>45</sup> reported that when the BCP chains are in contact with a corrugated substrate, the chain deformations are very different in the two  $L_{\perp}$  orientations. For the  $L_{\perp}^1$ , the chains are oriented along the “smooth” surface direction and they are almost not deformed, while for the  $L_{\perp}^2$

phase, the chains follow the contour of the substrate corrugation. This means that for the latter  $L_{\perp}^2$  phase the chains are locally extended or compressed, which costs more energy.<sup>46,47</sup>

Furthermore, as can also be seen in Figure 7, increasing the substrate roughness (decreasing  $L_s \sim q_s^{-1}$  in Figure 7) causes  $\Delta F$  to increase. This means that the  $L_{\perp}^1$  phase becomes more stable than the  $L_{\perp}^2$  phase as a function of  $q_s R$ . This tendency can be understood in terms of the loss of entropy that is more pronounced in the  $L_{\perp}^2$  phase than in the  $L_{\perp}^1$  phase.<sup>33</sup> Moreover, Figure 8 shows that a substrate with weak preference can limit the perpendicular domains around the crests of the substrate corrugation, resulting in a less random orientation than for a neutral substrate at early times. This facilitates the merging of perpendicular lamellae to form a single defect-free domain on a large length scale. We argue that the local film thickness is an important factor in obtaining the coexistence of parallel and perpendicular lamellar phases at early times. If the film thickness at the corrugation crests is too thick, it may form parallel (instead of perpendicular) lamellae at early times. In our simulations, the local film thickness at the corrugation crests is  $0.65L_0$  and  $1.15L_0$  in the valleys. While further simulations to identify the precise range of the local film thickness will be presented in a future work, in the present work we show strong evidence suggesting that the substrate roughness and weak preference have a synergy effect. This synergy greatly facilitates the stability of in-plane defect-free perpendicular lamellar phases. We note that in a recent study,<sup>48</sup> the surface weak preference was also determined to be a crucial factor in obtaining the orthogonal orientation with respect to the corrugation.

The advantage of the weak segregation regime (small  $N\chi_{AB}$ ) of the BCP film is that defects are not necessarily metastable but spontaneously convert into defect-free structures at low  $N\chi_{AB}$  (less than  $N\chi_{AB} = 18$ ).<sup>49</sup> After equilibration, one can use thermal annealing to lower the temperature toward the desired strong segregation regime, while maintaining a perfect alignment.

An interesting direction of extending the present study is to consider BCP blends. In experiments,<sup>34</sup> such blends cast on rough substrates have been shown to enhance the ordering of defect-free phases. We hope to further explore such films composed of BCP blends, given their great value in applications.

To the best of our knowledge, using the synergy between unidirectional corrugated substrates and a small preference field to produce defect-free phases has not yet been tested in experiments. Future experimental verifications of these scenarios may bring us closer to producing large arrays of defect-free BCP structures, while employing simple and viable techniques.

## AUTHOR INFORMATION

### Corresponding Authors

\*E-mail andelman@post.tau.ac.il (D.A.).

\*E-mail manxk@buaa.edu.cn (X.M.).

### Notes

The authors declare no competing financial interest.

## ACKNOWLEDGMENTS

We thank M. Müller for useful comments and T. Russell for numerous suggestions and clarifications on the feasibility of

experimental setups. We are grateful to A. C. Shi for suggesting us to explore the structure evolution along the SCFT iteration time axis. This work was supported in part by Grant No. 21404003 and 21434001 of the National Natural Science Foundation of China (NSFC), and the joint NSFC-ISF Research Program, jointly funded by the NSFC under Grant No. 51561145002 and the Israel Science Foundation (ISF) under Grant No. 885/15. D.A. acknowledges the hospitality of the KITPC and ITP, Beijing, China, and partial support from the Israel Science Foundation (ISF) under Grant No. 438/12, the United States–Israel Binational Science Foundation (BSF) under Grant No. 2012/060, and a CAS President's International Fellowship Initiative (PIFI).

## REFERENCES

- (1) Bates, F. S.; Fredrickson, G. H. Block Copolymers: Designer Soft Materials. *Phys. Today* **1999**, *52*, 32.
- (2) Bates, F. S.; Schulz, M. F.; Khandpur, A. K.; Förster, S.; Rosedale, J. H.; Almdal, K.; Mortensen, K. Fluctuations, conformational asymmetry and block copolymer phase behaviour. *Faraday Discuss.* **1994**, *98*, 7.
- (3) Zheng, W.; Wang, Z.-G. Morphology of ABC Triblock Copolymers. *Macromolecules* **1995**, *28*, 7215.
- (4) Hermel, T. J.; Hahn, S. F.; Chaffin, K. A.; Gerberich, W. W.; Bates, F. S. Role of Molecular Architecture in Mechanical Failure of Glassy/Semicrystalline Block Copolymers: CEC vs CECEC Lamellae. *Macromolecules* **2003**, *36*, 2190.
- (5) Christodoulou, S.; Driva, P.; Iatrou, H.; Hadjichristidis, N. Synthesis and Micellization Behavior of Janus H-Shaped A2BC2 Terpolymers. *Macromolecules* **2008**, *41*, 2607.
- (6) Bates, F. S.; Hillmyer, M. A.; Lodge, T. P.; Bates, C. M.; Delaney, K. T.; Fredrickson, G. H. Multiblock Polymers: Panacea or Pandora's Box? *Science* **2012**, *336*, 434.
- (7) Xiang, H.; Shin, K.; Kim, T.; Moon, S.; McCarthy, T. J.; Russell, T. P. The influence of confinement and curvature on the morphology of block copolymers. *J. Polym. Sci., Part B: Polym. Phys.* **2005**, *43*, 3377.
- (8) Shi, A.-C.; Li, B. H. Self-assembly of diblock copolymers under confinement. *Soft Matter* **2013**, *9*, 1398.
- (9) Luo, M.; Epps, T. H., III Directed Block Copolymer Thin Film Self-Assembly: Emerging Trends in Nanopattern Fabrication. *Macromolecules* **2013**, *46*, 7567.
- (10) Kim, H.-C.; Park, S.-M.; Hinsberg, W. D. Block Copolymer Based Nanostructures: Materials, Processes, and Applications to Electronics. *Chem. Rev.* **2010**, *110*, 146.
- (11) Herr, D. J. C. Directed block copolymer self-assembly for nanoelectronics fabrication. *J. Mater. Res.* **2011**, *26*, 122.
- (12) Kim, S. O.; Solak, H. H.; Stoykovich, M. P.; Ferrier, N. J.; de Pablo, J. J.; Nealey, P. F. Epitaxial self-assembly of block copolymers on lithographically defined nanopatterned substrates. *Nature* **2003**, *424*, 411.
- (13) Stoykovich, M. P.; Müeller, M.; Kim, S. O.; Solak, H. H.; Edwards, E. W.; de Pablo, J. J.; Nealey, P. F. Directed Assembly of Block Copolymer Blends into Nonregular Device-Oriented Structures. *Science* **2005**, *308*, 1442.
- (14) Man, X. K.; Andelman, D.; Orland, H. Block copolymer films with free interfaces: Ordering by nanopatterned substrates. *Phys. Rev. E* **2012**, *86*, 01801.
- (15) Park, S.-M.; Stoykovich, M. P.; Ruiz, R.; Zhang, Y.; Black, C. T.; Nealey, P. E. Directed Assembly of Lamellae-Forming Block Copolymers by Using Chemically and Topographically Patterned Substrates. *Adv. Mater.* **2007**, *19*, 607.
- (16) Li, H.; Huck, W. Ordered Block-Copolymer Assembly Using Nanoimprint Lithography. *Nano Lett.* **2004**, *4*, 1633.
- (17) Thébault, P.; Niedermayer, S.; Landis, S.; Chaix, N.; Guenoun, P.; Daillant, J.; Man, X.-K.; Andelman, D.; Orland, H. Tailoring Nanostructures Using Copolymer Nanoimprint Lithography. *Adv. Mater.* **2012**, *24*, 1952.
- (18) Sinturel, C.; Morris, V. M.; Hillmyer, M. A. Solvent Vapor Annealing of Block Polymer Thin Films. *Macromolecules* **2013**, *46*, 5399.
- (19) Nunns, A.; Gwyther, J.; Manners, I. Inorganic block copolymer lithography. *Polymer* **2013**, *54*, 1269.
- (20) Hamley, I. W. Ordering in thin films of block copolymers: Fundamentals to potential applications. *Prog. Polym. Sci.* **2009**, *34*, 1161.
- (21) Khanna, V.; Cochran, E. W.; Hexemer, A.; Stein, G. E.; Fredrickson, G. H.; Kramer, E. J.; Li, X.; Wang, J.; Hahn, S. F. Effect of Chain Architecture and Surface Energies on the Ordering Behavior of Lamellar and Cylinder Forming Block Copolymers. *Macromolecules* **2006**, *39*, 9346.
- (22) Sivaniah, E.; Hayashi, H.; Iino, M.; Hashimoto, T. Observation of Perpendicular Orientation in Symmetric Diblock Copolymer Thin Films on Rough Substrates. *Macromolecules* **2003**, *36*, 5894.
- (23) Sivaniah, E.; Hayashi, H.; Matsubara, S.; Kiyono, S.; Hashimoto, T.; Fukunaga, K.; Kramer, E. J.; Mates, T. Symmetric Diblock Copolymer Thin Films on Rough Substrates. Kinetics and Structure Formation in Pure Block Copolymer Thin Films. *Macromolecules* **2005**, *38*, 1837.
- (24) Bitá, I.; Yang, J. K. W.; Jung, Y. S.; Ross, C. A.; Thomas, E. L.; Berggren, K. K. Graphoepitaxy of Self-Assembled Block Copolymers on Two-Dimensional Periodic Patterned Templates. *Science* **2008**, *321*, 939.
- (25) Liu, P.-H.; Thébault, P.; Guenoun, P.; Daillant, J. Easy Orientation of Diblock Copolymers on Self-Assembled Monolayers Using UV Irradiation. *Macromolecules* **2009**, *42*, 9609.
- (26) Kulkarni, M. M.; Yager, K. G.; Sharma, A.; Karim, A. Combinatorial Block Copolymer Ordering on Tunable Rough Substrates. *Macromolecules* **2012**, *45*, 4303.
- (27) Kim, T.; Wooh, S.; Son, J. G.; Char, K. Orientation Control of Block Copolymer Thin Films Placed on Ordered Nanoparticle Monolayers. *Macromolecules* **2013**, *46*, 8144.
- (28) Bates, C. M.; Maher, M. J.; Janes, D. W.; Ellison, C. J.; Willson, C. G. Block Copolymer Lithography. *Macromolecules* **2014**, *47*, 2.
- (29) Vega, D. A.; Gómez, L. R.; Pezzutti, A. D.; Pardo, F.; Chaikin, P. M.; Register, R. A. Coupling between mean curvature and textures in block copolymer thin films deposited on curved substrates. *Soft Matter* **2013**, *9*, 9385.
- (30) Aissou, K.; Shaver, J.; Fleury, G.; Pecastaings, G.; Brochon, C.; Navarro, C.; Grauby, S.; Rampoux, J.-M.; Dilhaire, S.; Hadziioannou, G. Nanoscale Block Copolymer Ordering Induced by Visible Interferometric Micropatterning: A Route towards Large Scale Block Copolymer 2D Crystals. *Adv. Mater.* **2013**, *25*, 213.
- (31) Park, S.-M.; Berry, B. C.; Dobisz, E.; Kim, H.-C. Observation of surface corrugation-induced alignment of lamellar microdomains in PS-*b*-PMMA thin films. *Soft Matter* **2009**, *5*, 957.
- (32) Park, S.; Lee, D. H.; Xu, J.; Kim, B.; Hong, S. W.; Jeong, U.; Xu, T.; Russell, T. P. Macroscopic 10-Terabit-per-Square-Inch Arrays from Block Copolymers with Lateral Order. *Science* **2009**, *323*, 1030.
- (33) Hong, S. W.; Huh, J.; Gu, X.; Lee, D. H.; Jo, W. H.; Park, S.; Xu, T.; Russell, T. P. Unidirectionally aligned line patterns driven by entropic effects on faceted surfaces. *Proc. Natl. Acad. Sci. U. S. A.* **2012**, *109*, 1402.
- (34) Kim, B. H.; Choi, Y.; Kim, J. Y.; Shin, H.; Kim, S.; Son, S.-W.; Kim, S. O.; Kim, P. Wrinkle-Directed Self-Assembly of Block Copolymers for Aligning of Nanowire Arrays. *Adv. Mater.* **2014**, *26*, 4665.
- (35) Turner, M. S.; Joanny, J.-F. Diblock copolymer lamellae at rough surfaces. *Macromolecules* **1992**, *25*, 6681.
- (36) Tsori, Y.; Andelman, D. Parallel and Perpendicular Lamellae on Corrugated Surfaces. *Macromolecules* **2003**, *36*, 8560.
- (37) Tsori, Y.; Sivaniah, E.; Andelman, D.; Hashimoto, T. Orientational Transitions in Symmetric Diblock Copolymers on Rough Surfaces. *Macromolecules* **2005**, *38*, 7193.
- (38) Ranjan, A.; Kulkarni, M.; Karim, A.; Sharma, A. Diblock copolymer lamellae on sinusoidal and fractal surfaces. *J. Chem. Phys.* **2012**, *136*, 094903.

- (39) Ye, X.; Edwards, B. J.; Khomami, B. Block Copolymer Morphology Formation on Topographically Complex Surfaces: A Self-Consistent Field Theoretical Study. *Macromol. Rapid Commun.* **2014**, *35*, 702.
- (40) Man, X. K.; Tang, J. Z.; Zhou, P.; Yan, D. D.; Andelman, D. Lamellar Diblock Copolymers on Rough Substrates: Self-Consistent Field Theory Studies. *Macromolecules* **2015**, *48*, 7689.
- (41) Bosse, A. W.; García-Cervera, C. J.; Fredrickson, G. H. Microdomain Ordering in Laterally Confined Block Copolymer Thin Films. *Macromolecules* **2007**, *40*, 9570.
- (42) Hur, S.-M.; García-Cervera, C. J.; Kramer, E. J.; Fredrickson, G. H. SCFT Simulations of Thin Film Blends of Block Copolymer and Homopolymer Laterally Confined in a Square Well. *Macromolecules* **2009**, *42*, 5861.
- (43) Takahashi, H.; Laachi, N.; Delaney, K. T.; Hur, S.-M.; Weinheimer, C. J.; Shykind, D.; Fredrickson, G. H. Defectivity in Laterally Confined Lamella-Forming Diblock Copolymers: Thermodynamic and Kinetic Aspects. *Macromolecules* **2012**, *45*, 6253.
- (44) Kim, B. H.; Lee, H. M.; Lee, J.-H.; Son, S.-W.; Jeong, S.-J.; Lee, S.; Lee, D.; Kwak, S. U.; Jeong, H.; Shin, H.; Yoon, J.-B.; Lavrentovich, O. D.; Kim, S. O. Copolymer Film Alignment: Spontaneous Lamellar Alignment in Thickness-Modulated Block Copolymer Films. *Adv. Funct. Mater.* **2009**, *19*, 2584.
- (45) Pickett, G. T.; Witten, T. A.; Nagel, S. R. Equilibrium surface orientation of lamellae. *Macromolecules* **1993**, *26*, 3194.
- (46) Matsen, M. W.; Bates, F. S. Origins of complex self-Assembly in block copolymers. *Macromolecules* **1996**, *29*, 7641.
- (47) Pezzutti, A. D.; Gómez, L. R.; Vega, D. A. Smectic block copolymer thin films on corrugated substrates. *Soft Matter* **2015**, *11*, 2866.
- (48) Tavakkoli, K. G., A.; Nicaise, S. M.; Gadelrab, K. R.; Alexander-Katz, A.; Ross, C. A.; Berggren, K. K. Multilayer block copolymer meshes by orthogonal self-assembly. *Nat. Commun.* **2016**, *7*, 10518.
- (49) Li, W.; Nealey, P. F.; de Pablo, J. J.; Müller, M. Defect removal in the course of directed self-assembly is facilitated in the vicinity of the order-disorder transition. *Phys. Rev. Lett.* **2014**, *113*, 168301.